Chemical Geology xxx (xxxx) xxx–xxx

Contents lists available at ScienceDirect

Chemical Geology

journal homepage: www.elsevier.com/locate/chemgeo

Efficacy of in situ and meteoric ^{10}Be mixing in fluvial sediment collected from small catchments in China

Thomas B. Neilson[a], Amanda H. Schmidt[b,*], Paul R. Bierman[a], Dylan H. Rood[c,d,e], Veronica Sosa Gonzalez[f]

[a] Department of Geology, University of Vermont, 180 Colchester Ave., Burlington, VT 05405, USA
[b] Geology Department, Oberlin College, 403 Carnegie Building, 52 W. Lorain St., Oberlin, OH 44074, USA
[c] Department of Earth Science and Engineering, Imperial College London, South Kensington Campus, London SW7 2AZ, UK
[d] AMS Laboratory, Scottish Universities Environmental Research Centre, East Kilbride G75 0QF, UK
[e] Earth Research Institute, University of California, Santa Barbara, CA 93106, USA
[f] Rubenstein School of Environment and Natural Resources, University of Vermont, Burlington, VT 05405, USA

ARTICLE INFO

Editor: G. Jerome

Keywords:
Sediment mixing
Cosmogenic
Rivers
Sediment transport

ABSTRACT

Using measurements of *in situ* and meteoric ^{10}Be in fluvial sand to measure erosion rates, quantify soil loss, and trace sediment sources and sinks relies on the assumption that such sediment is well-mixed and representative of the upstream area. We test this assumption at 13 river junctions in three tributary watersheds (200–2500 km^2) to the Mekong River, Yunnan, China, where human alteration of the landscape is significant and widespread.

We find that two of the three watersheds mix well for *in situ* ^{10}Be and none mix well for meteoric ^{10}Be when considering the concentration of ^{10}Be at the outlet compared to the area-weighted mean of headwater samples. We also assessed mixing at 13 river junctions by comparing the erosion rate-weighted isotopic concentration of sediment taken from tributaries upstream of a junction to the concentration in a sample taken downstream of the junction. With this metric, mixing is generally poor for both *in situ* and meteoric ^{10}Be but is better for *in situ* ^{10}Be than for meteoric ^{10}Be ($p < 0.05$). This is likely because *in situ* ^{10}Be is measured in quartz, which is resilient to physical and chemical breakdown in river systems whereas meteoric ^{10}Be is measured in grain coatings which can abrade and dissolve.

Basins eroding faster (> 100 mm/kyr) tend to mix better than slowly eroding basins. We find no evidence that agricultural land use in sampled basins affects sediment mixing downstream. Mixing improves with increased basin area (particularly > 200 km^2), increased sampling distance downstream from an upstream junction (> 500 m), and increased difference in size between tributaries (one tributary > 3 times larger than the other). The most important factor affecting mixing efficacy for both *in situ* and meteoric ^{10}Be is the fraction of the basin area contributing to the downstream sample that does not contribute to the upstream samples. Junctions with > 2% of the basin area unsampled by upstream samples tend not to mix as well. Our data suggest specific sampling location strategies (such as amalgamation) likely to improve the outcome of fluvial network analysis using cosmogenic nuclides.

1. Introduction

Understanding the source and volume of sediment moving across the landscape, and the role of humans in sediment generation and transport, are fundamental issues in Earth science (NRC, 2012). To that end, isotopic measurements of in situ and meteoric ^{10}Be have been used repeatedly to quantify sediment generation and transport processes. For example, *in situ* ^{10}Be (^{10}Be$_i$), which forms in and is preferentially measured in quartz grains, is used to quantify basin-average erosion rates over 10^2–10^5 year timescales (e.g., Bierman and Steig, 1996; Brown et al., 1998; Brown et al., 1995; Granger et al., 1996; Harel et al., 2016; Hewawasam et al., 2003; Portenga and Bierman, 2011; Reusser et al., 2015; Vanacker et al., 2007).

Meteoric ^{10}Be (^{10}Be$_m$), which forms in the atmosphere, is delivered to sediment by precipitation and dryfall and is incorporated in grain-coatings. ^{10}Be$_m$ has been used to measure local soil transport rates (Jungers et al., 2009), basin-average erosion indices (a measure of soil loss) (Brown et al., 1988), trace sediment sources and sinks (Belmont

* Corresponding author.
E-mail address: aschmidt@oberlin.edu (A.H. Schmidt).

http://dx.doi.org/10.1016/j.chemgeo.2017.09.024
Received 5 June 2017; Received in revised form 4 August 2017; Accepted 17 September 2017

et al., 2014; Reusser and Bierman, 2010), and, more recently, to estimate basin-average erosion and weathering rates (Rahaman et al., 2017; Wittmann and von Blanckenburg, 2016; Wittmann et al., 2007). Underlying all such calculations with both $^{10}Be_i$ and $^{10}Be_m$ is the assumption that the sediment in rivers is well-mixed and representative of the entire upstream area (Bierman and Steig, 1996; Brown et al., 1995; Granger et al., 1996) without overrepresentation of some basin subregions (Carretier et al., 2015b; Safran et al., 2005).

^{10}Be derived erosion rates only represent an average of the entire contributing area if the sediment flux from contributing sub-basins is proportional to the long-term rate at which sediment is shed from the landscape in each basin (Bierman and Steig, 1996; Brown et al., 1995; Granger et al., 1996; von Blanckenburg et al., 2012). Sampling upstream and downstream of a junction allows testing of this assumption (Stone et al., 2006). For basins ranging in area from 10^0 to 10^6 km^2, prior work using $^{10}Be_i$ has found that the area-weighted mean erosion rate of tributary catchments converges on the erosion rate calculated from the $^{10}Be_i$ concentration in sediment at the basin outlet, suggesting that sediment is well-mixed (e.g., Bierman et al., 2005; Clapp et al., 2002; Matmon et al., 2003b; Portenga et al., 2015; Wittmann and von Blanckenburg, 2016; Wittmann et al., 2009). Conversely, poorly mixed sediment was identified at junctions in smaller (< 1–30 km^2) basins and generally attributed to insufficient sample collection distance downstream of the junction, stochastic sediment supply from tributaries (e.g., localized differences in precipitation or mass-wasting), and small catchment size (Binnie et al., 2006; Savi et al., 2014). In contrast, $^{10}Be_m$ mixing has not been tested, although Reusser and Bierman (2010) showed that $^{10}Be_m$ concentration increased downstream as sediment from less disturbed basins entered the system, suggesting that tributary sediment is mixing into the main stem channel sediment.

Sediment mixing is potentially affected by the location of sample sites (hereafter, termed *unmixed* above a junction and *mixed* below a junction), stochastic events, and human influence. Basin area contributing to the mixed sample can affect mixing because larger basins tend to have erosion rates that converge on the full basin average rate as determined from smaller subbasins (e.g., Clapp et al., 2002). The distance that the mixed sample was collected below the tributary junction can affect the apparent efficacy of mixing because too short a distance may limit the ability of the river to homogenize sediment from the tributaries (Binnie et al., 2006; Savi et al., 2014). The ratio of the larger upstream tributary area to the smaller upstream tributary area can affect mixing because relatively small tributaries entering relatively large rivers do not significantly increase channel sediment load (Benda et al., 2004), thus making it likely that sediment from tributaries that are more different in size will at least appear to be well mixed.

Different erosional processes determine the grain size of sediment leaving the watershed (Brown et al., 1995; Sosa Gonzalez et al., 2016), potentially resulting in a bias in mixing efficacy when only a specific grain size is sampled (Aguilar et al., 2014; Carretier et al., 2015a). The area contributing to the mixed sample, but not to the two unmixed samples (hereafter, termed *residual area*), could affect the modeled isotopic concentration of the mixed sample because sediment from this area is not measured in unmixed samples and this residual area may be eroding at a different rate than sampled upstream basins (Portenga et al., 2015).

Stochastic events, such as debris flows, can generate waves of sediment that take time to move down the fluvial system and overwhelm other sediment as they move through (Gran and Czuba, 2017; Miller and Benda, 2000; Sutherland et al., 2002). This would, in turn, affect sediment mixing because sampled sediment would predominantly come from the sediment wave (Kober et al., 2012; Savi et al., 2014) and might not reflect the long-term behavior (and isotopic character) of the entire upstream catchment.

Human activity can affect mixing in various ways. Difference in upstream agricultural land use between two basins could increase modern sediment yield relative to the long-term sediment generation rate (e.g., Covault et al., 2013; Regard et al., 2016; Reusser et al., 2015; Von Blanckenburg et al., 2004) and thus invalidate mixing model calculations. Conversely, dams will typically reduce the sediment yield from the dammed tributary (Syvitski et al., 2005; Walter and Merritts, 2008) similarly invalidating calculations based on isotopically determined erosion rates. Dams immediately upstream of sampling sites have been found to increase apparent erosion rates derived from $^{10}Be_i$ at sample sites because sediment is mostly sourced from areas between the dam and the sample collection site (Reusser et al., 2017).

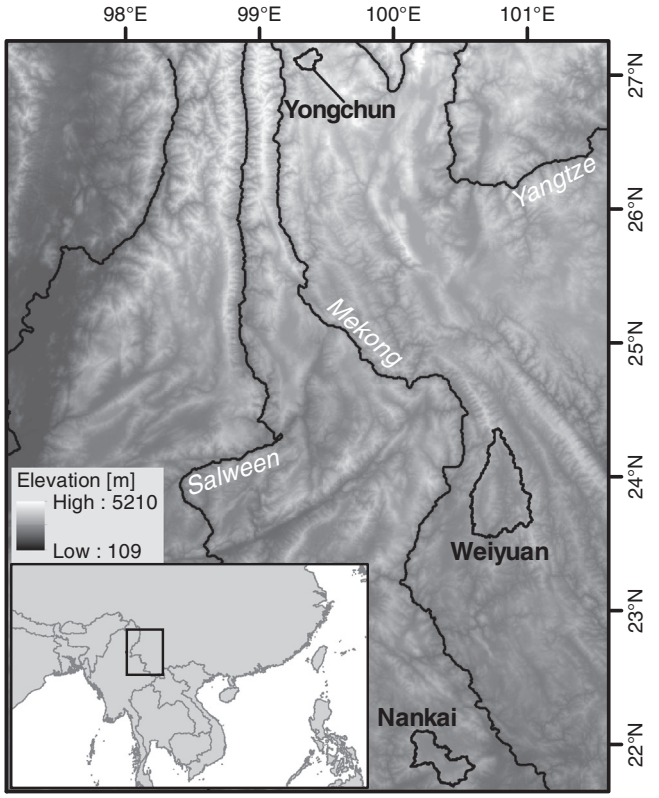

Fig. 1. Study location showing sampled basins, major regional rivers, and elevation (NASA LP-DAAC, 2012). Inset shows the region of interest within Southeast Asia.

Here, we test for thorough sediment mixing by measuring both $^{10}Be_m$ and $^{10}Be_i$ in three tributary watersheds to the Mekong River: the Yongchun (198 km^2), Weiyuan (2508 km^2), and Nankai (1006 km^2) (Fig. 1). We chose the Yongchun, Weiyuan, and Nankai Rivers based on the range in basin area, the gradient in agricultural land use, and the relative elevation of the basins. In this way, we are able to test if efficacy of mixing depends on human induced land-use change, topographic characteristics, or sampling site location (Fig. 2).

2. Field sites

The Yongchun watershed is a small (198 km^2), steep (mean slope = 19°), high-elevation watershed situated on the southeastern margin of the Tibetan plateau. In 2012, a large (~30 m tall) dam was completed in the southern arm of the Yongchun, and we observed numerous small diversion and check dams as well as out-of- and in-channel gravel mining operations. Land use in the basin consists primarily of forest, cultivated land on unterraced hillslopes, shrubland, and grassland. Although the rivers in the Yongchun watershed are relatively small, valley bottom rivers flow through Quaternary alluvium and are often braided. Headwater channels are steep with exposed bedrock. Wide-spread gravel mining has disturbed many rivers.

The Weiyuan basin is the largest of the three basins (2508 km^2) and lower in elevation than the Yongchun. Steep slopes (mean slope = 19°) generally prevail throughout the basin with gentle slopes limited to

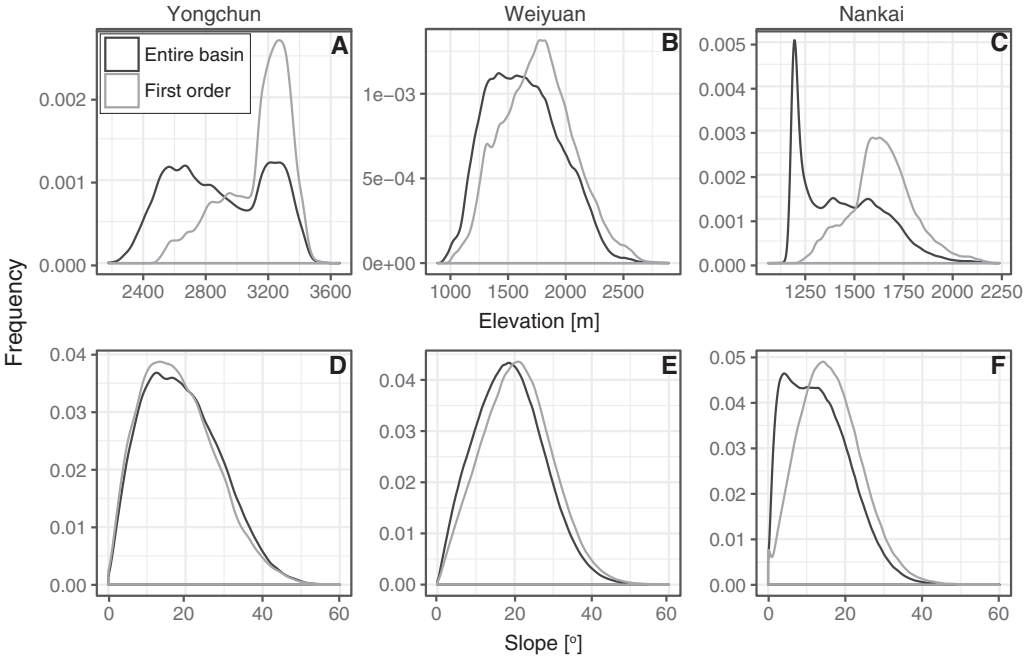

Fig. 2. Elevation (A, B, C) and slope (D, E, F) distributions for the outlet of the Yongchun (A, D), Weiyuan (B, E), and Nankai (C, F) basins and for the first order tributaries sampled (i.e., samples with no samples upstream of them).

valley floors. Land use in the basin is either forested or cultivated, with agriculture comprising ~22% of the total basin area, primarily in valley bottoms; hillslopes are generally not terraced. As with the Yongchun watershed, gravel mining is common in rivers throughout the watershed and headwater channels are steep with frequent bedrock exposures. Valley bottom channels are typically single thread.

The Nankai basin (1006 km^2) is the lowest elevation and furthest south of the three basins. Steep upland sub-basins and expansive low-slope valley floors characterize the Nankai (mean slope = 13°). The majority of streams are diverted near the mountain-front to irrigate sugarcane and rice paddies that cover the valley floor; the natural river channel in much of the northern arm is completely obscured by agriculture and irrigation structures. The landscape is primarily cultivated (~50%), with some forest (including rubber and tea plantations) and grassland. Although there is extensive terracing for valley bottom agriculture, hillslopes are generally not terraced. As with the other basins, gravel mining is widespread. The headwater rivers in the Nankai basin are steep, bedrock channels; lower elevation rivers are typically deeply incised in agricultural land or completely diverted for irrigation. For more details on spatial patterns of erosion in these watersheds, see Schmidt et al. (2016).

3. Methods

3.1. Sampling

We sampled detrital, active channel sediment at 54 sites in three watersheds in Yunnan, China (Fig. 3, Table S1), as described in Schmidt et al. (2016). These sites include 13 stream junctions with both unmixed incoming tributaries 53–3950 m (mean = 838 m, median = 459 m) above the junction and the mixed channel 104–7040 m (mean = 957 m, median = 358 m) downstream of the junction for a total of 37 samples (5 junctions in the Yongchun, 6 in the Weiyuan, and 2 in the Nankai; at one junction, three unmixed tributaries were sampled; 3 samples are downstream of one junction and upstream of another) (Fig. 4).

We collected samples of fluvial sediment from point bars, mid-channel islands, depositional pools, and channel beds in 2013 immediately prior to the start of the summer monsoon. Sample sites were evaluated in the field to account for intensive human alteration of the channel nearby, including sediment mining. If extensive human alteration was present, we moved sampling sites to a more suitable location (usually upstream). We field sieved sediment to 250–850 μm, the grain-size typically used for $^{10}Be_i$ analysis. $^{10}Be_m$ analysis was also performed on 250–850 μm sediment to ensure that both isotopic analyses used the same grain-size fraction, and thereby limiting the possibility for grain-size specific processes to complicate comparisons.

3.2. Laboratory procedures

3.2.1. $^{10}Be_i$

Bulk aliquots of each sample were purified to isolate quartz using chemical etching (Kohl and Nishiizumi, 1992) at the University of Vermont. Prior to Be extraction, the purity of isolated quartz was tested using inductively coupled plasma – optical emission spectroscopy. Be was extracted from ~5–25 g of purified quartz spiked with ~250 μg of ^{9}Be following established procedures (Corbett et al., 2016). Each batch of 12 included one process blank and one CRONUS N standard (Jull et al., 2015). For this project, we analyzed 7 standards that result in a population with a mean = 2.25×10^5 atoms/g, median = 2.23×10^5 atoms/g, and a coefficient of variation (COV) = 6.3% (Table S2a). We note that the 6.3% COV is about twice the precision of the individual sample isotopic measurements; the scatter above analytical uncertainty may reflect variations related to laboratory procedures and the loading of cathodes for AMS analysis or inhomogeneity of the material. We conclude that the 6.3% COV represents the actual reproducibility of our measurements and is closer to the true uncertainty in the isotopic concentrations. Below, we use twice the COV (2 sigma; 13%), rather than individual measurement precision, to test for the efficacy of mixing. $^{10}Be/^{9}Be$ ratios were measured by Accelerator Mass Spectrometry at the Scottish Universities Environmental Research Centre (Xu et al., 2010, 2015), normalized to the NIST standard with an assumed $^{10}Be/^{9}Be$ ratio of 2.79×10^{-11} (Nishiizumi et al., 2007), and background corrected by subtracting the average process blank ratio of $2.64 \pm 0.98 \times 10^{-15}$ (n = 7, 1 SD; ~1.11% of the mean sample ratio) from each sample ratio and propagating uncertainties in quadrature (Table S3). Erosion rates were calculated based on the $^{10}Be_i$ abundance in each sample, effective elevation (Portenga and Bierman, 2011), mean latitude, and mean longitude using the CRONUS-Earth online calculator (Accessed March 2014; main code v2.2, constants file

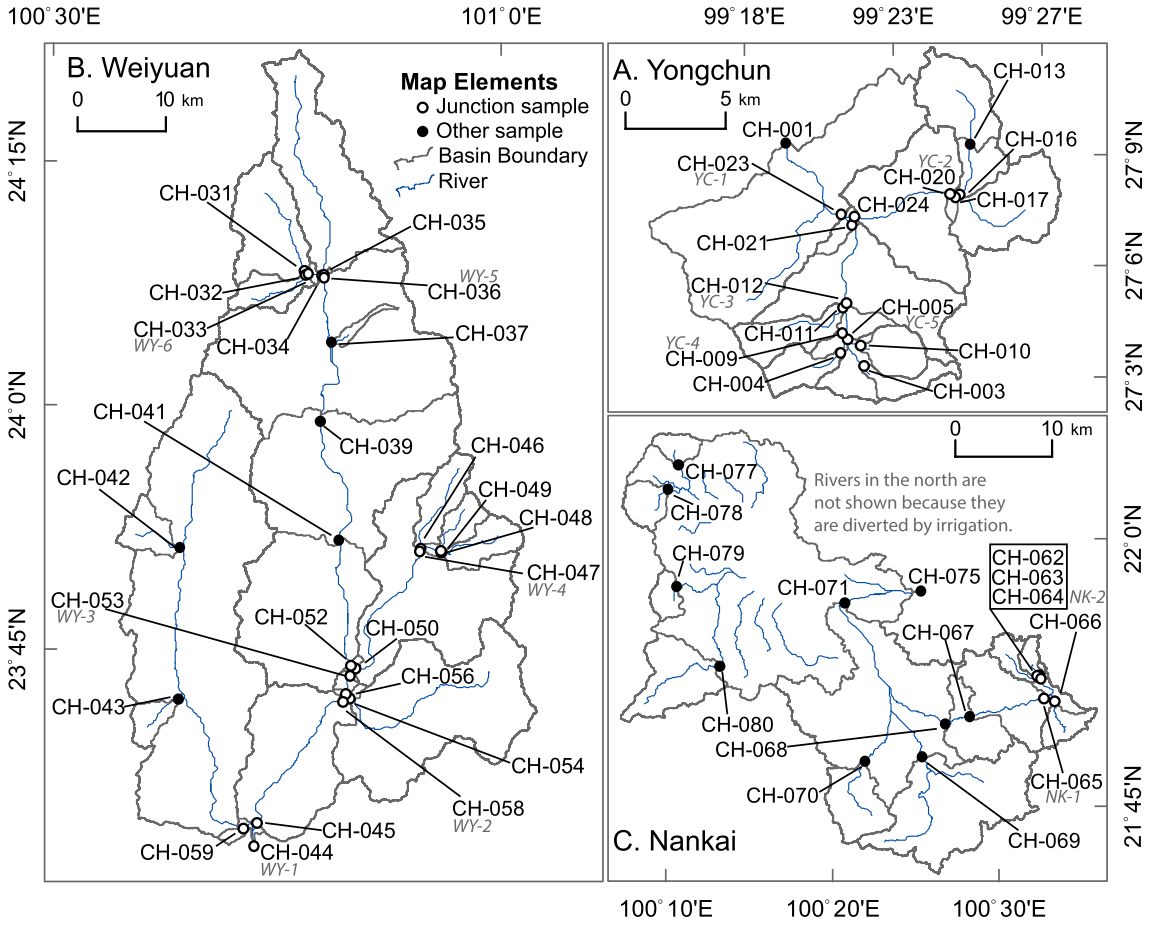

Fig. 3. Map shows the location, basin boundary, sample ID (in black) for each sample, and mixing junction ID (in grey near the downstream sample) for each junction in the Yongchun (a), Weiyuan (b), and Nankai (c). Note that no rivers are mapped in the lowlands of the north Nankai subbasin because it the river is entirely diverted for irrigation. Samples in junction analyses are shown with white circles while other samples are black circles. Data shown in this figure are in table S1 (for sample locations) and table S6 (for junction IDs and samples contributing).

v2.2.1, time invariant global production rate, and the Lal/Stone scaling scheme (Lal, 1991; Stone, 2000), Table S4) (Balco et al., 2008). Effective elevation was calculated by determining the elevation required for a sample taken at the mean basin latitude and longitude to have the same production rate as the mean production rate of every pixel in the basin upstream of the sample site.

3.2.2. $^{10}Be_m$

At the University of Vermont we dried and powdered samples, then extracted Be from ~0.5 g of sample adding ~300–400 μg of ^{9}Be carrier using a modification of the fusion method presented by Stone (1998). ^{10}Be/^{9}Be ratios were measured and blank-corrected following the same method as used for $^{10}Be_i$, except that one process blank was run with each batch of 15 unknowns. Sample ratios were blank-corrected using

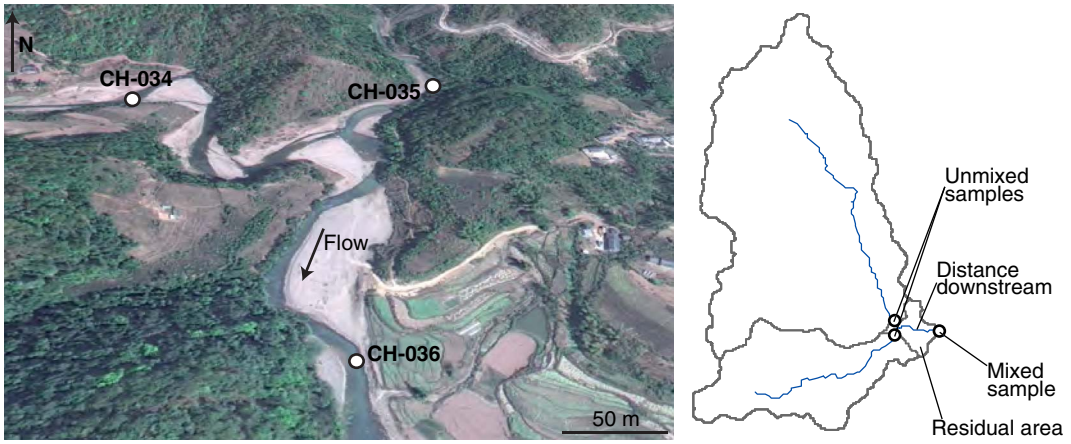

Fig. 4. Satellite image showing junction WY-5 in the Weiyuan Basin. Arrow shows flow direction and circles mark sample locations. CH-035 is 90 m upstream of the junction. CH-034 is 260 m upstream of the junction. CH-036 is 340 m downstream of the junction. The image is from Google Earth. To the right is a schematic showing terms we use to describe junctions and the samples taken at them.

the mean blank value of $2.28 \pm 2.31 \times 10^{-14}$ (n = 6, 1 SD), which is ~2% of the mean sample ratio (Table S3). For this set of samples we did not run a standard with our analyses, but for other samples from the same project we ran the STA1(KFA) standard with five batches of samples (Sosa Gonzalez et al., 2017). The mean concentration of $^{10}Be_m$ in these standards is $1.07 \pm 0.04 \times 10^8$ atoms/g (n = 5, 1 SD), which is a COV of 3.5%, which is again approximately double analytical precision for individual measurements. Other analyses of STA1(KFA) processed at UVM and analyzed at SUERC replicate with a similar COV. As with calculations for $^{10}Be_i$, we use 2xCOV of the standard (~7%) as the uncertainty in samples rather than the reported analytical uncertainty.

3.3. Digital data

We use 30 m resolution digital elevation models generated by NASA and METI's ASTER GDEM program (NASA LP-DAAC, 2012) as the basis for calculating basin boundaries and upstream areas. We measured distance from junctions using Google Earth to estimate actual river distance. Land-use data is from the GLC30 land cover dataset and represents 30 m resolution land cover from 2010 derived from Landsat TM, ETM+, and Chinese HJ-1 multispectral satellite images and a suite of auxiliary data sources (Chen et al., 2015).

3.4. Sediment mixing

We assess sediment mixing in two different ways. 1) For each of the three watersheds, we consider whether with increasing basin area, the furthest downstream sample has a similar erosion rate to the area-weighted mean erosion rate of zero order (i.e., no samples upstream) tributary basins (Bierman et al., 2005; Clapp et al., 2002; Matmon et al., 2003b; Wittmann et al., 2009) (see Fig. 4 for slope and elevation distributions of the entire watershed and first order watersheds for each basin). 2) We assess sediment mixing by measuring each isotope in sediment from the unmixed contributing streams above the junction as well as in mixed sediment collected downstream of the junction (Binnie et al., 2006; Savi et al., 2014).

To assess whether sediment is mixed at each junction, we use the simple linear mixing model described by Binnie et al. (2006). Possible ranges of acceptable mixing are based on the sediment yield (from the ^{10}Be-determined erosion rate) for each unmixed sample. Modeled downstream concentration ranges linearly from 100% contribution of one sample to 100% contribution of the other sample on a plot of isotopic concentration as a function of the fraction of sediment contributed by one unmixed sample. The intersection of measured and modeled concentration gives the range of possible contribution from the upstream tributary. If this is within the possible range based on measured sediment yields, the sample is well mixed. If the downstream measured concentration is within error of all measured unmixed samples, it is impossible to assess whether the junction is well-mixed. Thus, we report junctions as "well-mixed", "poorly mixed", or "cannot test".

To quantify degree of mixing at each junction, for each isotope, the upstream concentrations are used to model the concentration downstream of the junction, $\overline{N}$, using the area and erosion rate weighted average (Eq. (1)):

$$\overline{N} = \frac{\sum N_j E_j A_j}{\sum E_j A_j}, \quad (1)$$

where N_j is the nuclide concentration of upstream sample j, E_j is the $^{10}Be_i$–derived erosion rate, and A_j is the area (Granger et al., 1996). For $^{10}Be_m$ mixing we also use Eq. (1), substituting the $^{10}Be_m$ concentration for N_j and continuing to use $^{10}Be_i$-derived erosion rates for E_j. We then calculate the percent difference, D, from the measured sample downstream as follows:

$$D = \left(\frac{\overline{N} - N_{meas}}{N_{meas}}\right) \times 100 \quad (2)$$

where $\overline{N}$ is the modeled concentration downstream of the junction and N_{meas} is the measured concentration downstream of the junction.

When testing whether mixing is different for $^{10}Be_i$ and $^{10}Be_m$, we use a Wilcoxon signed-rank test (a paired difference test). The null hypothesis for the test is that the two sets of samples are drawn from the same population and the alternate hypothesis is that the samples are from different populations; thus, the p-value returned is the probability that the sample populations are the same. In this case, we compare the absolute value of the percent difference (D from Eq. (2)) of pairs of samples because the goal is to quantify how different they are from each other rather than whether they are above or below 0. We then normalize the data to account for the different lab replicability of the two Be isotopic systems (2σ = 13% for $^{10}Be_i$ and 7% for $^{10}Be_m$). To do this, we divide the absolute value of each sample pair's percent difference by the 2σ value (i.e., D divided by 13 for $^{10}Be_i$ and D divided by 7 for $^{10}Be_m$).

4. Results

4.1. Basin mixing

The erosion rate converges on the area-weighted mean of the zero-order watersheds concentration for the Weiyuan and Nankai watersheds, but not for the Yongchun (Fig. 5 A, C, E). This indicates that sediment mixing is sufficient for estimating $^{10}Be_i$ erosion rates at least in larger basins (Bierman et al., 2005; Matmon et al., 2003a; Wittmann et al., 2007). However, $^{10}Be_m$ concentration at the outlet does not converge on the mean for any watersheds (Fig. 5 B, D, F); both the Yongchun and Weiyuan outlet sediments have significantly lower $^{10}Be_m$ concentrations than the tributary average while the Nankai has much higher $^{10}Be_m$ concentration.

4.2. Junction mixing

Using $^{10}Be_i$, we find that sediment is well mixed at only 3 of 13 junctions (Fig. 6); an additional 3 junctions have upstream concentrations too similar to assess mixing. One sample from each watershed mixes well for $^{10}Be_i$. In general, samples with lower $^{10}Be_i$ concentrations tend to mix better than samples with higher concentrations (Fig. 7a). The percent difference between measured and modeled concentrations downstream scatters around zero (inset histograms, Fig. 7a) so there is no bias, just noise.

Sediment mixing measured with $^{10}Be_m$ displays similar trends to $^{10}Be_i$, though with differing magnitudes (Fig. 6). We find that two junctions are well-mixed using $^{10}Be_m$; an additional two cannot be tested because unmixed samples have concentrations too similar to each other and the measured mixed sample and the remaining junctions are poorly mixed. As with $^{10}Be_i$, samples with lower $^{10}Be_m$ concentration tend to mix better than those with higher concentrations (Fig. 7b). In contrast to $^{10}Be_i$, poorly mixed junctions are skewed to having higher modeled than measured $^{10}Be_m$ (inset histograms, Fig. 7b). Although only one fewer junction mixes well for $^{10}Be_m$ than $^{10}Be_i$, $^{10}Be_i$ mixes better than $^{10}Be_m$, as determined by a Wilcoxon-signed Rank Test ($p < 0.05$).

5. Discussion

For the Chinese drainage basins that we study here, we find that $^{10}Be_i$ mixes well at the basin scale for larger basins (> 200 km^2) but that $^{10}Be_m$ does not. Both isotopes are generally poorly mixed when considering junction mixing. Below we explore possible reasons that $^{10}Be_i$ and $^{10}Be_m$ mix differently. We then consider four primary controls on the efficacy of sediment mixing below stream junctions for both

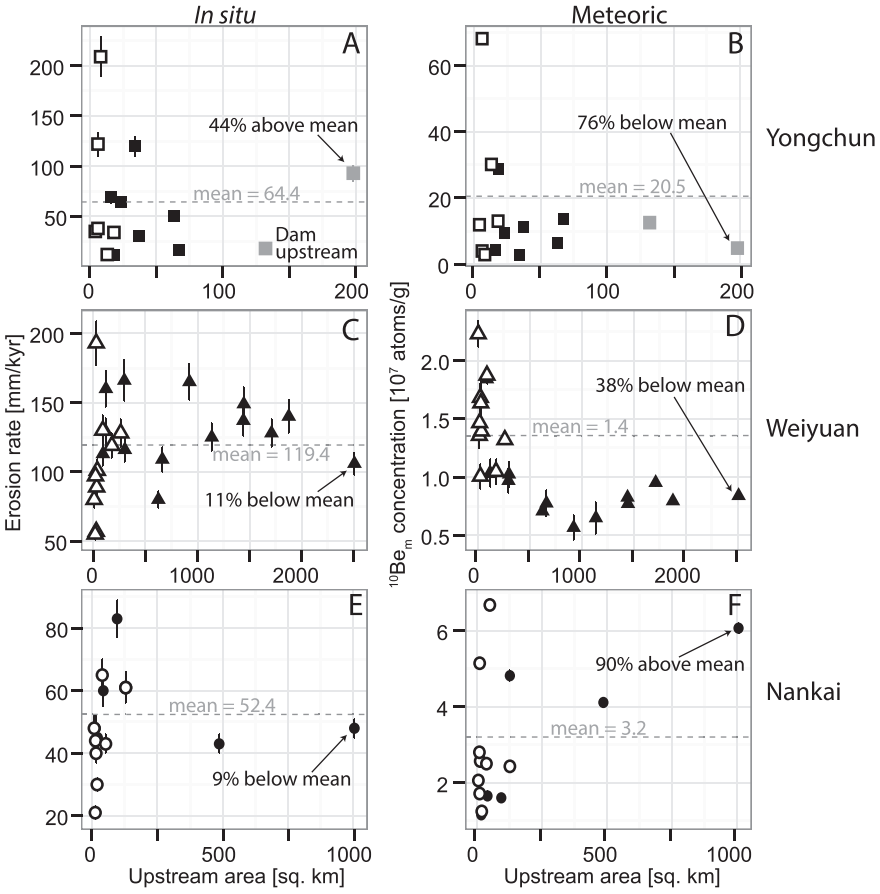

Fig. 5. Plots showing the $^{10}Be_i$ erosion rate (A, C, E) and $^{10}Be_m$ concentration (B, D, F) as a function of upstream area for the Yongchun (A, B), Weiyuan (C, D), and Nankai (E, F) watersheds. Dashed grey line on each plot represents the area weighted mean erosion rate or $^{10}Be_m$ concentration of all zero-order samples in the watershed (i.e., no samples upstream). Zero-order samples are shown with hollow shapes while filled shapes are higher order tributary samples. Error bars are shown as 1 SD of analytical uncertainty. Samples collected below junction YC-1, which are grey, are downstream of a dam. The percent differences from the mean are calculated as: Ratio = $^{10}Be_{sample}/^{10}Be_{mean}$; values > 1 are reported as % Difference = (Ratio − 1) × 100 "above mean"; values < 1 are reported as % Difference = Ratio × 100 "below mean". Data in this figure can be found in table S5.

$^{10}Be_i$ and $^{10}Be_m$: isotopic concentration of the downstream sample, sample site location, human influence, and stochastic events. By considering individual junctions in detail, we understand better what affects mixing efficacy. We conclude by offering recommendations for sampling strategies based on these observations.

5.1. Why do $^{10}Be_i$ and $^{10}Be_m$ mix differently?

Our results suggest that $^{10}Be_i$ mixes better than $^{10}Be_m$ at both the watershed and junction scale. Different mixing efficacy for these two systems has important implications for using them together to unravel both erosion and weathering rates (Wittmann et al., 2015), as they likely represent or at least are biased toward different parts of the drainage basin fluvial sediment transport system. We are not aware of other studies assessing $^{10}Be_m$ mixing at junctions, but there are data from other studies that allow analysis of watershed-scale mixing (i.e., comparing the concentration of the outlet sample to the area-weighted concentration of zero-order headwater samples). Adding data from three prior studies to our new data finds somewhat contradictory results concerning the trends of $^{10}Be_m$ from upstream to downstream in river systems (Brown et al., 1988; Rahaman et al., 2017; Wittmann et al., 2015). We find that in 4 of 8 watersheds where this analysis is possible (n = 3 from this study, n = 5 from previously published studies), the downstream concentration is lower than the area-weighted mean upstream concentration (Table 1); in the remaining four the downstream concentration is higher. The watershed in China with a higher downstream concentration is the Nankai basin, which drains extensive rice paddies where sediment may be stored and accumulate $^{10}Be_m$.

Another test of $^{10}Be_m$ consistency over space and time is the change in isotopic concentration at multiple points along a single river. Using a series of 6 samples taken along the main stem of the Salween River (Sosa Gonzalez et al., 2017), the $^{10}Be_m$ concentration of active channel sediments increases with distance downstream ($p < 0.01$), but the concentration in overbank sediments deposited during the previous years' monsoon does not ($p = 0.14$).

There is no clear explanation for why $^{10}Be_i$ and $^{10}Be_m$ mix differently (Fig. 7); however, it is likely that this is a result of the differences in the isotopic systems. $^{10}Be_i$ is produced and measured in quartz, an abundant and stable component of most river sediment. In contrast, $^{10}Be_m$ concentrations in river sediment are the result of a complex pedogenic biogeochemical system and the isotope is carried in grain coatings (Barg et al., 1997) which may not be transported conservatively downstream. In other words, the stability of $^{10}Be_m$ in the river system may be less than $^{10}Be_i$; $^{10}Be_m$ is likely a non-conservative tracer in some river systems, such as those with aggregate grains as described below. Here, we measured $^{10}Be_m$ on grains in the 250–850 μm grain size fraction. However, in our samples, this grain size fraction contained aggregate grains cemented by Fe and clay (Singleton et al., 2017). It is possible that these aggregate grains contain proportionately more of the total $^{10}Be_m$ than single grains (Wittmann et al., 2012), and are less stable than quartz sand. Disaggregation of sediment grains over short distances (i.e. between upstream and downstream samples) (Dyer and Olley, 1999) or mechanical abrasion of grain-coatings, which contain most of the $^{10}Be_m$ (Greene, 2016; Singleton et al., 2017) would cause non-conservative behavior of $^{10}Be_m$, resulting in less accurate mixing models. Evidence for such non-conservative behavior of $^{10}Be_m$ is the decreasing concentration of $^{10}Be_m$ as watershed size increases for both the Yongchun and the Weiyuan watersheds (Fig. 5) and that mixed samples tend to have higher measured than modeled $^{10}Be_m$ concentrations (Fig. 7). We do not see this behavior in the Nankai watershed, but have only two downstream samples, so it is hard to draw conclusions from such a small population.

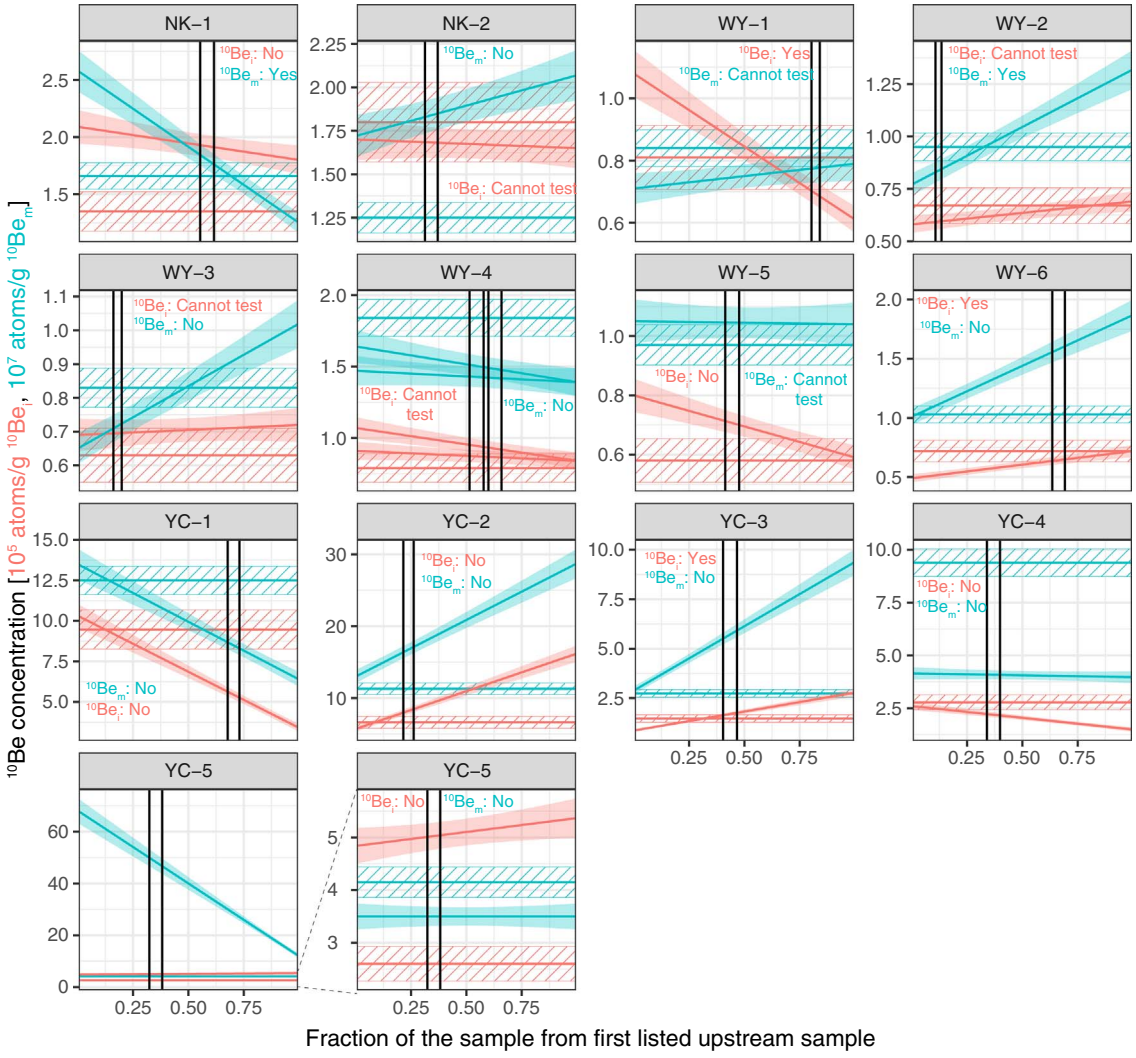

Fig. 6. Results of the mixing model for all junctions. Teal represents results for $^{10}Be_m$ and red represents results for $^{10}Be_i$. Black vertical lines are the range of contributions of the upstream basin based on sediment yield from contributing watersheds. Solid filled areas are the possible mixes of downstream sediment based on the upstream contributing watersheds. The hash-filled area is the measured downstream isotopic concentration with error bars (7% for $^{10}Be_m$, 13% for $^{10}Be_i$). Each junction is labeled at the top of the plot. For WY-4, there are three unmixed samples contributing to one mixed sample, so the mixing model is shown with two solid areas, each representing a pair of the upstream samples. The actual mix of three samples will be in the range of areas filled by the two-part mixing models. If the hashed area overlaps with the solid fill area between the two black lines, the sample is well-mixed. If the hashed area overlaps with the solid fill area for all mixes of sediment, we cannot determine if the sample is well-mixed. If the hashed area overlaps with the solid fill area outside the vertical black lines or does not overlap at all, the sample is poorly mixed. (For interpretation of the references to color in this figure legend, the reader is referred to the web version of this article.)

5.2. Isotopic concentration of downstream sample

We observe that junctions with lower isotopic concentrations downstream of the junction tend to be better mixed than junctions with higher isotopic concentrations (Fig. 8). $^{10}Be_i$ concentration is inversely proportional to erosion rate (Bierman and Steig, 1996; Brown et al., 1995; Granger et al., 1996) and proportional to the elevation at which the quartz was exposed at and near the surface (Lal, 1991; Stone, 2000). Thus, we consider erosion rate of the downstream basin here instead of $^{10}Be_i$ concentration as a factor which may affect mixing efficacy. $^{10}Be_m$ concentration is also inversely proportional to erosion rate (von Blanckenburg et al., 2012) but is not elevation dependent (Graly et al., 2011). However, because the relationship between erosion and $^{10}Be_m$ is not yet well understood and subject to greater uncertainty and many more assumptions than the $^{10}Be_i$ system, we do not consider erosion rates derived from $^{10}Be_m$ (Greene, 2016; von Blanckenburg et al., 2012; Willenbring and von Blanckenburg, 2010).

Although mixing efficacy for $^{10}Be_i$ is not correlated with erosion rate of the downstream sample (Fig. 8A), the mean erosion rate of well mixed $^{10}Be_i$ junctions is higher than the mean erosion rate of poorly mixed junctions (mean erosion = 120 mm/kyr, standard deviation = 12 mm/kyr, n = 3 for well mixed junctions; mean erosion = 61 mm/kyr, standard deviation = 52 mm/kyr, n = 6 for poorly mixed junctions; Fig. 9A). Similarly, mixing efficacy for $^{10}Be_m$ is not correlated with the $^{10}Be_m$ concentration of the downstream sample (Fig. 8B) but the mean $^{10}Be_m$ concentration of well mixed junctions is lower than that of poorly mixed junctions (mean $^{10}Be_m$ concentration = 1.31×10^7 atoms/g for well mixed junctions and 2.74×10^7 atoms/g for poorly mixed junctions; Fig. 9B). Lower $^{10}Be_m$ concentration implies higher rates of erosion in the upstream watershed (von Blanckenburg et al., 2012).

Thus, it seems that when erosion rates in the upstream catchments are higher and fluxes of sediment greater, mixing improves. Specifically, we find that all junctions where upstream basins are eroding faster than 100 mm/kyr mix well for $^{10}Be_i$ and all junctions where the downstream sample has $^{10}Be_m$ concentration below 1×10^7 atoms/g mix well for $^{10}Be_m$. It may be that sediment mixes better when larger fluxes of sediment are moving through the river system.

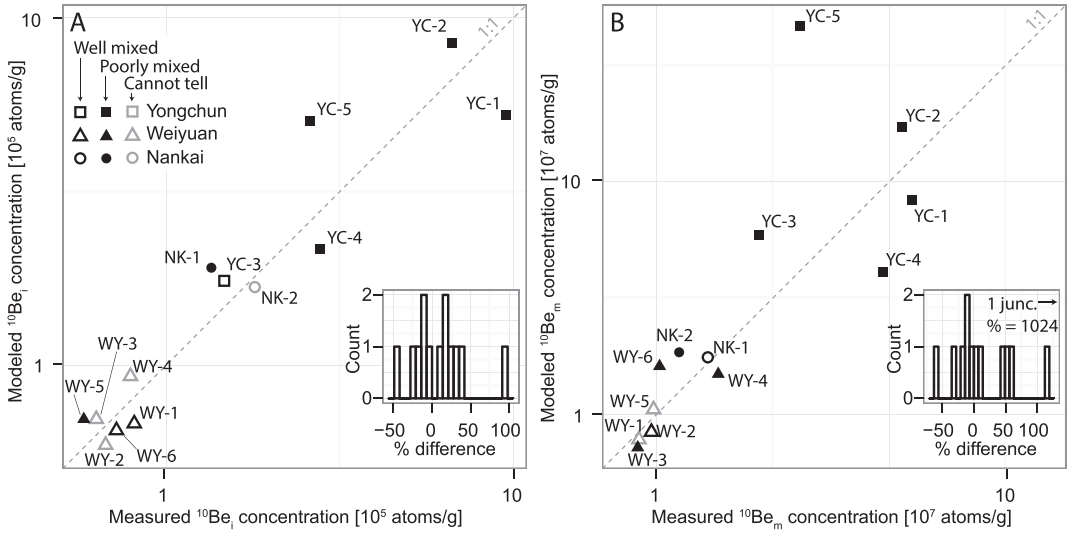

Fig. 7. Log-log plots showing the downstream measured and modeled concentrations (Eq. (1)) of $^{10}Be_i$ (A) and $^{10}Be_m$ (B) at each junction. The 1-1 line on each plot represents perfect mixing. Sample mixing is assessed based on Fig. 6. Insets show histograms of the distribution of the data. Histogram bins are 7%. Data shown in this figure are in table S6.

Table 1
Summary of data showing area-weighted mean headwater concentration of $^{10}Be_m$ compared to the measured concentration of a sample downstream of all headwater samples.

Study	Watershed	Area-weighted average upstream concentration (10^7 atoms/g)[a]	Downstream concentration (10^7 atoms/g)
This study – China	Yongchun	20.5 ± 22.6 (n = 6)	4.85 ± 0.16
	Weiyuan	1.4 ± 0.35 (n = 10)	0.84 ± 0.03
	Nankai	3.2 ± 1.65 (n = 9)	6.07 ± 0.14
Wittmann et al. (2015) – Amazon	Amazon	3.49 ± 6.51 (n = 9)	1.62 ± 0.07
Brown et al. (1988) – Eastern US	Susquehanna	17.5 ± 8.00 (n = 3)	31.1 ± 7.15
	Neuse	69.9 ± 33.2 (n = 3)	19.3 ± 4.44
	Coal	25.0 ± 8.10 (n = 2)	41.4 ± 9.52
Rahaman et al. (2017) – Ganges	Ganges	7.21 ± 7.06 (n = 6)	9.70 ± 0.19

[a] Error is the standard deviation of the averaged concentrations.

5.3. Sample site location

For the influence of sample site location on mixing efficacy, we consider four possible factors: basin area of the mixed sample, residual unsampled area (Fig. 4), the distance the mixed sample is from the junction, and relative size of tributaries upstream. We find that the greater the difference in basin area between the mixed sample site and the total area of unmixed samples relative to the total area of the watershed sampled (i.e., the residual area), the greater the disagreement between modeled and measured ^{10}Be concentrations (Fig. 8C, D). However, we do not see a difference in the fraction residual area between well mixed and poorly mixed samples (Fig. 9C, D). For both isotopes, the correlation between the absolute value of the difference in measured and modeled isotopic concentration as a function of fraction residual area is significant ($p < 0.01$) and explains a large fraction of the variance in the data ($R^2 \geq 0.77$). In other words, the larger the area sampled by the mixed sample that is not included in the unmixed samples, the greater the proportion of the landscape that is unsampled and thus not considered in the mixing model (Portenga et al., 2015).

We also find that mixing efficacy is generally better for larger basins (Figs. 8E, F and 9E, F), especially for $^{10}Be_m$. In both cases, the median size of basins that mix well is significantly higher than that of basins that do not mix well (Fig. 8E, F). Most junctions where we can assess mixing with upstream basins over 150 km^2 are well mixed for both $^{10}Be_i$ and $^{10}Be_m$. This is likely because these basins have more channel distance in which to mix and higher discharge with which to mix sediment. In addition, individual stochastic events are less likely to affect ^{10}Be concentrations in larger basins (Niemi et al., 2005), supporting previous findings that over a certain basin area, samples tend to be well mixed (Bierman et al., 2005; Clapp et al., 2002; Matmon et al., 2003b; Portenga et al., 2015; Wittmann et al., 2009).

Similarly, as others have found (Binnie et al., 2006; Savi et al., 2014), it seems that when samples are taken farther downstream, mixing efficacy improves (Fig. 8G, H), although this seems to be more important for $^{10}Be_m$ (Fig. 9G, H). Most junctions where we can assess mixing and where the downstream sample was over 500 m downstream of the junction are well mixed for both isotopes. Distance downstream will only improve mixing up to a threshold, beyond which increasing distance results in too great an increase in residual area to the total area sampled, decreasing the apparent mixing efficacy. In this sense, residual area may provide a more meaningful metric by which to assess ideal mixed sample location. In combination, distance downstream of a junction should be maximized as long as the residual area does not exceed ~2% of the area upstream of the downstream sample.

Finally, mixing efficacy improves the larger the difference in upstream area between the tributaries (Fig. 8I, J), although for very large differences in tributary areas, it may not be possible to resolve mixing. One much larger tributary increases mixing efficacy because the larger tributary dominates the sediment load and the other tributary is contributing relatively little sediment to the total load (Miller and Benda, 2000). Contrast in tributary basin size seems to be a more sensitive factor in mixing for $^{10}Be_i$ than $^{10}Be_m$ (Fig. 9I, J). For the junctions we

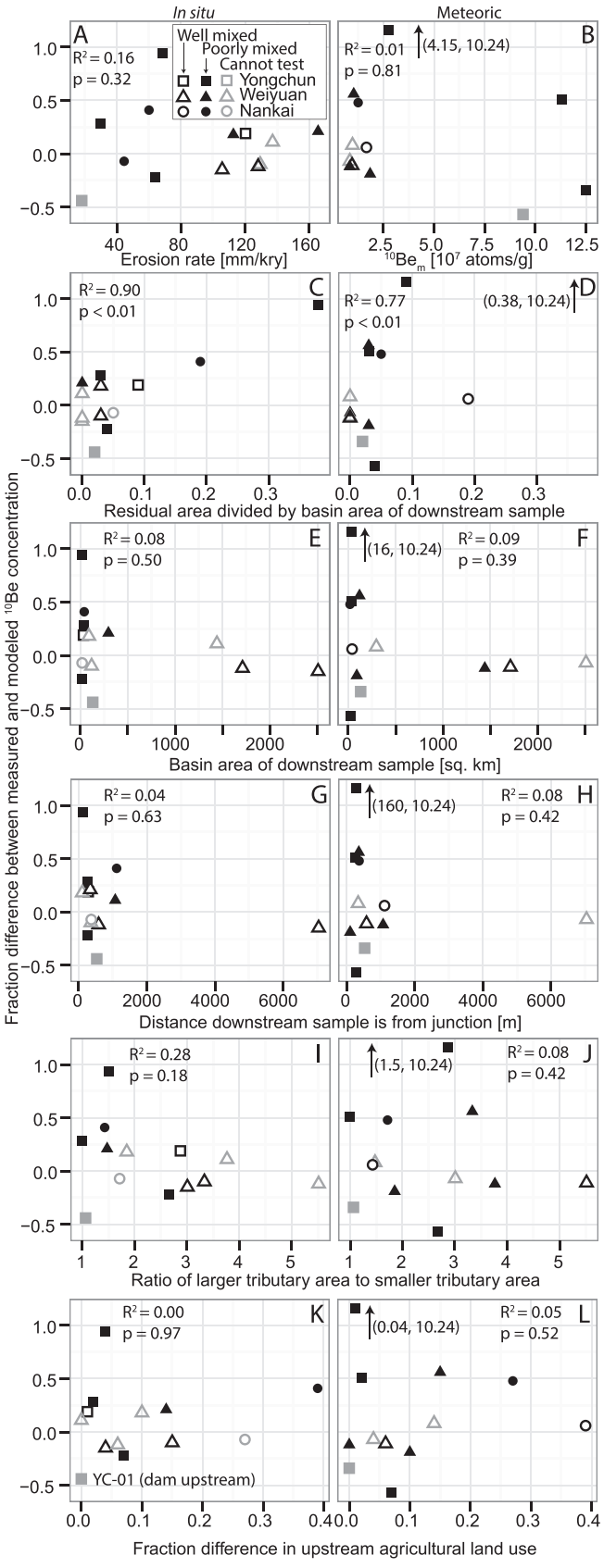

Fig. 8. The fraction difference between measured and modeled isotopic concentrations (Eq. (2)) for $^{10}Be_i$ (A, C, E, G, I, K) and $^{10}Be_m$ (B, D, F, H, J, L) as a function of the difference in erosion rate of the downstream sample (A), $^{10}Be_m$ concentration of the downstream sample (B), residual area divided by basin area of mixed sample (C, D), basin area of the downstream sample (E, F), distance the mixed sample is from the junction (G, H), the ratio of the larger to the smaller tributary upstream of the junction (I, J), and the difference in agricultural land between the two tributary basins (K, L). In the case where there are three tributaries coming together, the ratio is of the largest to the smallest. The junction downstream of a major dam is shown with a grey square; this junction is left out of correlation analyses. Junctions which are considered to be well mixed are shown as outlines, junctions which are considered to be poorly mixed are solid black, junctions which are ambiguous are shown in grey outline (these junctions are left out of correlation analyses). Correlation statistics reported in each plot are for the absolute value of the fraction difference between the measured and modeled ^{10}Be concentrations. Data shown in this figure are in table S6.

sampled, all basins where we can assess mixing and where one tributary is at least 3 times the upstream area of the other mix well for $^{10}Be_i$ and but only one mixes well for $^{10}Be_m$.

5.4. Human activity

Human activity has both altered land use and channels in the field area (Schmidt et al., 2016). We found no robust relationship between sediment mixing efficacy at junctions and land-use metrics of basins upstream (Figs. 8K, L and 9K, L). In contrast, a large dam directly above a tributary junction (Junction ID YC-1) significantly reduced sediment supplied by that tributary to sample site CH-021, thus altering the isotopic composition of CH-021 to disproportionately reflect the other tributary above the junction (Figs. 5 and 6). This effect on isotope concentration has been noted in other regions where dams are common (Reusser et al., 2017).

5.5. Stochastic events

Stochastic events that deliver large quantities of sediment from a small portion of the landscape could affect sediment mixing (e.g., Binnie et al., 2006; Godard et al., 2012; Savi et al., 2014). We observed no evidence of significant landslides in the field and precipitation is primarily delivered by monsoons (Henck et al., 2010) that affect all field sites. Thus, we consider stochastic events such as very large landslides (e.g., Binnie et al., 2006; Godard et al., 2012; Savi et al., 2014) an unlikely explanation of poor mixing in our field area but they are important elsewhere, especially in steep, tectonically active terrain.

5.6. Sampling strategies

Our data suggest that sampling strategies can minimize noise and maximize mixing in samples, especially in areas heavily affected by human modifications of the landscape or which are slowly eroding. One strategy is to aggregate samples taken from several sites in the same general area (e.g., Carretier et al., 2013; Nichols et al., 2002), thereby manually mixing sediment from the sample site. Beyond amalgamating samples, our data suggest that in humid regions, noise will be reduced for basin areas > 200 km^2, a sampling distance of at least 500 m below junctions, and when the larger tributary at a junction is at least three times the upstream area of the smaller (Fig. 10). In addition, we find that when residual area is > 2% of the downstream basin area, samples are likely to appear poorly mixed due to the contribution of sediment from the residual area. This suggests that a residual area of at least 2% is required to infer erosion rates of the unsampled area between samples (e.g., Granger et al., 1996; Portenga et al., 2015). Finally, because basins eroding faster than 100 mm/kyr and with $^{10}Be_m$ concentrations below 10^7 atom/g were more likely to be well-mixed in our study, when sampling river sediment in slowly eroding regions, it is especially important to amalgamate sediment and to ensure samples are taken in locations that are more likely to be well-mixed.

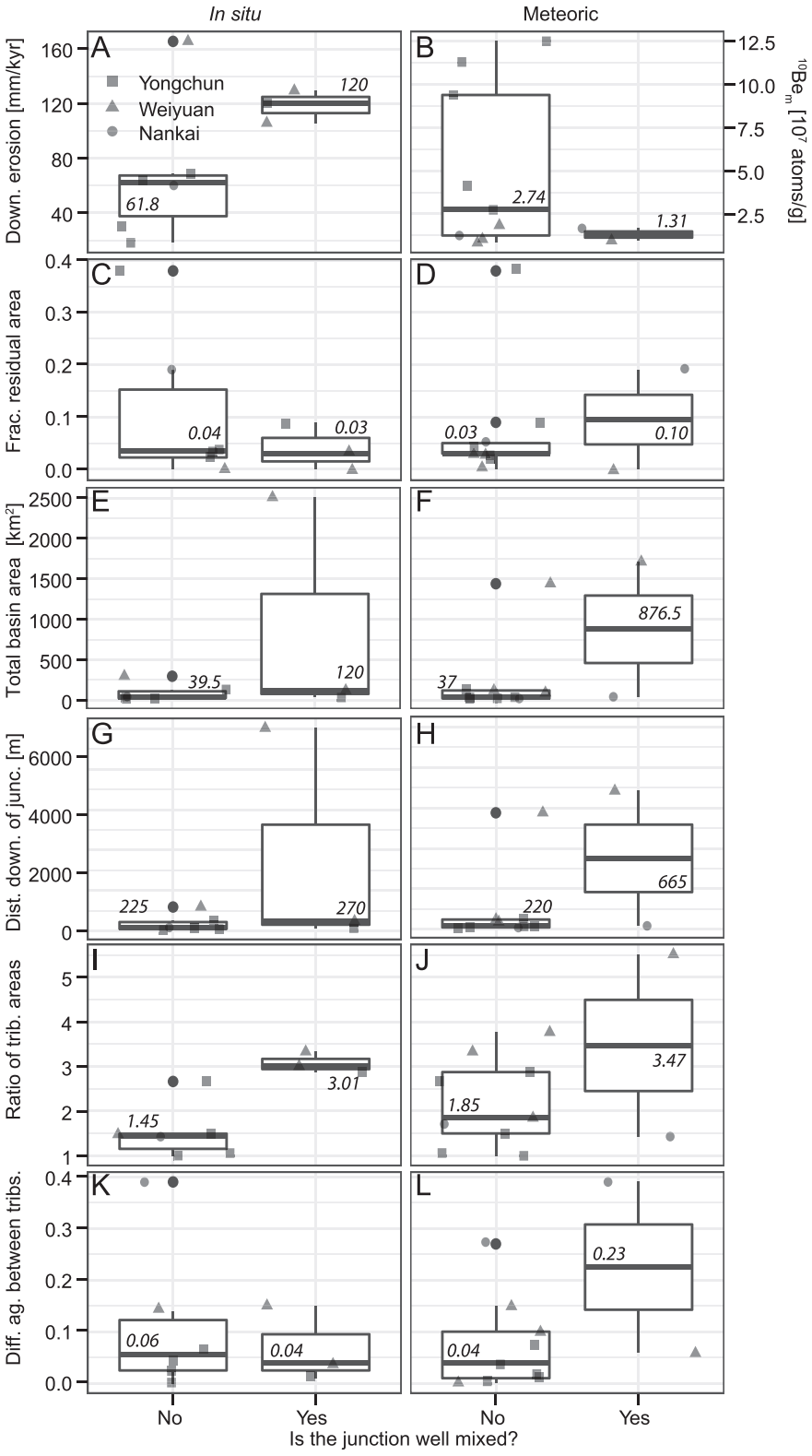

Fig. 9. Box plots showing the distribution of parameters for junctions where the junction is well mixed (for definition of "well mixed", see methods) for $^{10}Be_i$ (A, C, E, G, I, K) and $^{10}Be_m$ (B, D, F, H, J, L). For boxplots, the median is the middle line, the 25th and 75th percentiles are the edges, and whiskers extend to include all samples within 1.5 times the range of the box; outliers fall outside this range. Grey points are data summarized by boxplots. Italicized text in or near boxes is the median value for the box. Only junctions that are clearly mixed or not mixed are shown; unclear junctions are not shown.

6. Conclusions

We tested the assumption that detrital sediment is well mixed using $^{10}Be_i$ and $^{10}Be_m$ for three watersheds in Yunnan, China. For these watersheds (16 to 2500 km^2), we find that isotopic concentration of samples converge on the average of sample concentrations for zero-order tributaries as upstream area increases for $^{10}Be_i$ but not $^{10}Be_m$; this pattern suggests that other factors, likely related to the instream instability of aggregate grains and grain coatings, affect $^{10}Be_m$ mixing and transport. In addition, we find that mixing at individual junctions is generally poor for both $^{10}Be_i$ and $^{10}Be_m$. The fraction of the downstream basin not sampled in the upstream samples is the most important factor in whether junctions appear well mixed. In addition, sediment mixing is better for more rapidly eroding watersheds, basins > 200 km^2, when

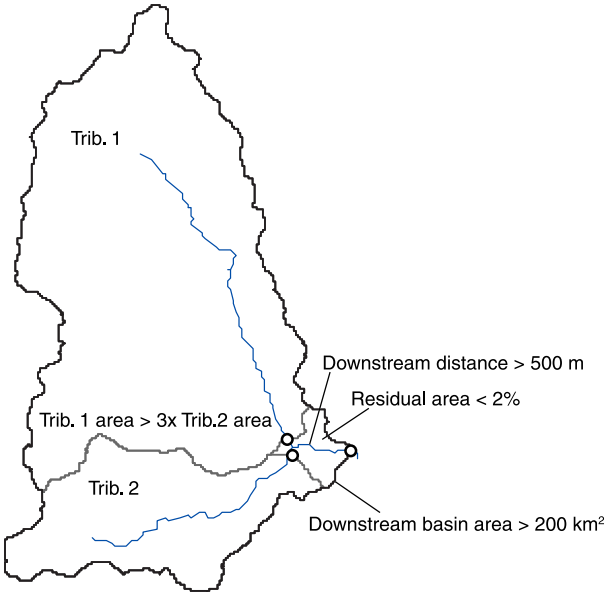

Fig. 10. Summary of sampling recommendations to maximize the chance that the sample is well-mixed and representative of the entire upstream area when samples are taken downstream of tributary junctions. Residual area only matters if junction mixing efficacy is being tested or if one is trying to infer the erosion rate of an unsampled region (in which case the residual area should exceed 2%).

one tributary is much larger than another, and when sampling distance is far enough downstream to ensure adequate distance for sediment to mix. To reduce the noise in erosion rates determined from *in situ* ^{10}Be measured in river sediment, we suggest sampling at least several hundred meters downstream of tributary junctions, amalgamating samples from multiple locations in the channel, and sampling larger rather than smaller basins.

Acknowledgements

Research supported by NSF awards EAR-1114166 (to Schmidt), EAR-1114159 (to Bierman), and EAR-1114436 (to Rood). We thank staff of the AMS Laboratory at the Scottish Universities Environmental Research Centre (SUERC) for support during ^{10}Be measurements. We thank C. M. Zhang, R. J. Wei, and J. A. Bower for field assistance and V. Regard, G. Balco, and an anonymous reviewer for constructive feedback on early versions of the manuscript. Data used in this paper are included as tables in the supplemental information.

Appendix A. Supplementary data

Supplementary data to this article can be found online at https://doi.org/10.1016/j.chemgeo.2017.09.024.

References

Aguilar, G., Carretier, S., Regard, V., Vassallo, R., Riquelme, R., Martinod, J., 2014. Grain size-dependent ^{10}Be concentrations in alluvial stream sediment of the Huasco Valley, a semi-arid Andes region. Quat. Geochronol. 19, 163–172.

Balco, G., Stone, J.O., Lifton, N.A., Dunai, T.J., 2008. A complete and easily accessible means of calculating surface exposure ages or erosion rates from ^{10}Be and ^{26}Al measurements. Quat. Geochronol. 3, 174–195.

Barg, E., Lal, D., Pavich, M.J., Caffee, M.W., Southon, J.R., 1997. Beryllium geochemsitry in soils; evaluation of ^{10}Be/^{9}Be ratios in authigenic minerals as a basis for age models. Chem. Geol. 140, 237–258.

Belmont, P., Willenbring, J., Schottler, S., Marquard, J., Kumarasamy, K., Hemmis, J., 2014. Toward generalizable sediment fingerprinting with tracers that are conservative and nonconservative over sediment routing timescales. J. Soils Sediments 14, 1479–1492.

Benda, L., Andras, K., Miller, D., Bigelow, P., 2004. Confluence effects in rivers: interactions of basin scale, network geometry, and disturbance regimes. Water Resour. Res. 40.

Bierman, P.R., Steig, E., 1996. Estimating rates of denudation and sediment transport using cosmogenic isotope abundances in sediment. Earth Surf. Process. Landf. 21, 125–139.

Bierman, P.R., Reuter, J.M., Pavich, M., Gellis, A.C., Caffee, M.W., Larsen, J., 2005. Using cosmogenic nuclides to contrast rates of erosion and sediment yield in a semi-arid, arroyo-dominated landscape, Rio Puerco Basin, New Mexico. Earth Surf. Process. Landf. 30, 935–953.

Binnie, S.A., Phillips, W.M., Summerfield, M.A., Fifield, L.K., 2006. Sediment mixing and basin-wide cosmogenic nuclide analysis in rapidly eroding mountainous environments. Quat. Geochronol. 1, 4–14.

von Blanckenburg, F., Bouchez, J., Wittmann, H., 2012. Earth surface erosion and weathering from the ^{10}Be (meteoric)/^{9}Be ratio. Earth Planet. Sci. Lett. 351–352, 295–305.

Brown, L., Pavich, M., Hickman, R.E., Klein, J., Middleton, R., 1988. Erosion of the eastern United States observed with ^{10}Be. Earth Surf. Process. Landf. 13, 441–457.

Brown, E.T., Stallard, R.F., Larsen, M.C., Raisbeck, G.M., Yiou, F., 1995. Denudation rates determined from the accumulation of *in situ*-produced ^{10}Be in the Luquillo experimental forest, Puerto Rico. Earth Planet. Sci. Lett. 129, 193–202.

Brown, E.T., Stallard, R.F., Larsen, M.C., Bourles, D.L., Raisbeck, G.M., Yiou, F., 1998. Determination of predevelopment denudation rates of an agricultural watershed (Cayaguas River, Puerto Rico) using *in-situ*-produced ^{10}Be in river-borne quartz. Earth Planet. Sci. Lett. 160, 723–728.

Carretier, S., Regard, V., Vassallo, R., Aguilar, G., Martinod, J., Riquelme, R., Pepin, E., Charrier, R., Hérail, G., Farías, M., 2013. Slope and climate variability control of erosion in the Andes of central Chile. Geology 41, 195–198.

Carretier, S., Regard, V., Vassallo, R., Aguilar, G., Martinod, J., Riquelme, R., Christophoul, F., Charrier, R., Gayer, E., Farías, M., 2015a. Differences in ^{10}Be concentrations between river sand, gravel and pebbles along the western side of the central Andes. Quat. Geochronol. 27, 33–51.

Carretier, S., Regard, V., Vassallo, R., Martinod, J., Christophoul, F., Gayer, E., Audin, L., Lagane, C., 2015b. A note on ^{10}Be-derived mean erosion rates in catchments with heterogeneous lithology: examples from the western Central Andes. Earth Surf. Process. Landf. 40, 1719–1729.

Chen, J., Chen, J., Liao, A., Cao, X., Chen, L., Chen, X., He, C., Han, G., Peng, S., Lu, M., Zhang, W., Tong, X., Mills, J., 2015. Global land cover mapping at 30 m resolution: a POK-based operational approach. ISPRS J. Photogramm. Remote Sens. 103, 7–27.

Clapp, E., Bierman, P.R., Caffee, M., 2002. Using ^{10}Be and ^{26}Al to determine sediment generation rates and identify sediment source areas in an arid region drainage basin. Geomorphology 45, 89–104.

Corbett, L.B., Bierman, P.R., Rood, D.H., 2016. An approach for optimizing *in situ* cosmogenic ^{10}Be sample preparation. Quat. Geol. 33, 24–34.

Covault, J.A., Craddock, W.H., Romans, B.W., Fildani, A., Gosai, M., 2013. Spatial and temporal variations in landscape evolution: historic and longer-term sediment flux through global catchments. J. Geol. 121, 35–56.

Dyer, F.J., Olley, J.M., 1999. The effects of grain abrasion and disaggregation on ^{137}Cs concentrations in different size fractions of soils developed on three different rock types. Catena 36, 143–151.

Godard, V., Burbank, D.W., Bourlès, D.L., Bookhagen, B., Braucher, R., Fisher, G.B., 2012. Impact of glacial erosion on ^{10}Be concentrations in fluvial sediments of the Marsyandi catchment, central Nepal. J. Geophys. Res. Earth 117, F03013.

Graly, J.A., Reusser, L.J., Bierman, P.R., 2011. Short and long-term delivery rates of meteoric ^{10}Be to terrestrial soils. Earth Planet. Sci. Lett. 302, 329–336.

Gran, K.B., Czuba, J.A., 2017. Sediment pulse evolution and the role of network structure. Geomorphology 277, 17–30.

Granger, D.E., Kirchner, J.W., Finkel, R., 1996. Spatially averaged long-term erosion rates measured from *in situ*-produced cosmogenic nuclides in alluvial sediments. J. Geol. 104, 249–257.

Greene, E.S., 2016. Comparing meteoric ^{10}Be, in situ ^{10}Be, and native ^{9}Be across a diverse set of watersheds. In: Geology. University of Vermont, Burlington, VT, pp. 118.

Harel, M.-A., Mudd, S., Attal, M., 2016. Global analysis of the stream power law parameters based on worldwide ^{10}Be denudation rates. Geomorphology.

Henck, A.C., Montgomery, D.R., Huntington, K.W., Liang, C., 2010. Monsoon control of effective discharge, Yunnan and Tibet. Geology 38, 975–978.

Hewawasam, T., von Blackenburg, F., Schaller, M., Kubik, P., 2003. Increase of human over natural erosion rates in tropical highlands constrained by cosmogenic nuclides. Geology 31, 597–600.

Jull, A.J.T., Scott, E.M., Bierman, P., 2015. The CRONUS-Earth inter-comparison for cosmogenic isotope analysis. Quat. Geochronol. 26, 3–10.

Jungers, M.C., Bierman, P.R., Matmon, A., Nichols, K., Larsen, J., Finkel, R., 2009. Tracing hillslope sediment production and transport with *in situ* and meteoric ^{10}Be. J. Geophys. Res. 114, 1–16.

Kober, F., Hippe, K., Salcher, B., Ivy-Ochs, S., Kubik, P.W., Wacker, L., Hahlen, N., 2012. Debris-flow-dependent variation of cosmogenically derived catchment-wide denudation rates. Geology 40, 935–938.

Kohl, C.P., Nishiizumi, K., 1992. Chemical isolation of quartz for measurement of *in-situ*-produced cosmogenic nuclides. Geochim. Cosmochim. Acta 56, 3583–3587.

Lal, D., 1991. Cosmic-ray labeling of erosion surfaces — in situ nuclide production-rates and erosion models. Earth Planet. Sci. Lett. 104, 424–439.

Matmon, A., Bierman, P.R., Larsen, J., Southworth, S., Pavich, M., Caffee, M., 2003a. Temporally and spatially uniform rates of erosion in the southern Appalachian Great Smoky Mountains. Geology 31, 155–158.

Matmon, A.S., Bierman, P., Larsen, J., Southworth, S., Pavich, M., Finkel, R., Caffee, M., 2003b. Erosion of an ancient mountain range, the Great Smoky Mountains, North Carolina and Tennessee. Am. J. Sci. 303, 817–855.

Miller, D.J., Benda, L.E., 2000. Effects of punctuated sediment supply on valley-floor landforms and sediment transport. Geol. Soc. Am. Bull. 112, 1814–1824.

NASA LP-DAAC, 2012. ASTER GDEM. In: NASA Land Processes Distributed Active Archive Center (LP DAAC). LP DAAC.
Nichols, K.K., Bierman, P.R., Hooke, R.L., Clapp, E.M., Caffee, M., 2002. Quantifying sediment transport on desert piedmonts using Be-10 and Al-26. Geomorphology 45, 105–125.
Niemi, N.A., Oskin, M., Burbank, D.W., Heimsath, A.J.M., Gabet, E.J., 2005. Effects of bedrock landslides on cosmogenically determined erosion rates. Earth Planet. Sci. Lett. 237, 480–498.
Nishiizumi, K., Imamura, M., Caffee, M.W., Southon, J.R., Finkel, R.C., McAninch, J., 2007. Absolute calibration of ^{10}Be AMS standards. Nucl. Inst. Methods Phys. Res. B 258, 403–413.
NRC, 2012. New Research Opportunities in the Earth Sciences. National Academy Press, Washington, DC.
Portenga, E.W., Bierman, P.R., 2011. Understanding Earth's eroding surface with ^{10}Be. GSA Today 21, 4–10.
Portenga, E.W., Bierman, P.R., Duncan, C., Corbett, L.B., Kehrwald, N.M., Rood, D.H., 2015. Erosion rates of the Bhutanese Himalaya determined using in situ-produced ^{10}Be. Geomorphology 233, 112–126.
Rahaman, W., Wittmann, H., von Blanckenburg, F., 2017. Denudation rates and the degree of chemical weathering in the Ganga River basin from ratios of meteoric cosmogenic ^{10}Be to stable ^{9}Be. Earth Planet. Sci. Lett.
Regard, V., Carretier, S., Boeglin, J.L., Ndam Ngoupayou, J.R., Dzana, J.G., Bedimo Bedimo, J.P., Riotte, J., Braun, J.J., 2016. Denudation rates on cratonic landscapes: comparison between suspended and dissolved fluxes, and ^{10}Be analysis in the Nyong and Sanaga River basins, South Cameroon. Earth Surf. Process. Landf. 41, 1671–1683.
Reusser, L.J., Bierman, P.R., 2010. Using meteoric ^{10}Be to track fluvial sand through the Waipaoa River basin, New Zealand. Geology 38, 47–50.
Reusser, L.J., Bierman, P., Rood, D., 2015. Quantifying human impacts on rates of erosion and sediment transport at a landscape scale. Geology 43, 171–174.
Reusser, L.J., Bierman, P.R., Rizzo, D.M., Portenga, E.W., Rood, D.H., 2017. Characterizing landscape-scale erosion using ^{10}Be in detrital fluvial sediment: slope-based sampling strategy detects the effect of widespread dams. Water Resour. Res. 53.
Safran, E.B., Bierman, P.R., Aalto, R., Dunne, T., Whipple, K.X., Caffee, M., 2005. Erosion rates driven by channel network incision in the Bolivian Andes. Earth Surf. Process. Landf. 30, 1007–1024.
Savi, S., Norton, K., Picotti, V., Brardinoni, F., Akçar, N., Kubik, P.W., Delunel, R., Schlunegger, F., 2014. Effects of sediment mixing on ^{10}Be concentrations in the Zielbach catchment, central-eastern Italian Alps. Quat. Geochronol. 19, 148–162.
Schmidt, A.H., Neilson, T.B., Bierman, P.R., Rood, D.H., Ouimet, W.B., Sosa Gonzalez, V., 2016. Influence of topography and human activity on apparent in situ ^{10}Be-derived erosion rates in Yunnan, SW China. Earth Surf. Dyn. 4, 819–830.
Singleton, A.A., Schmidt, A.H., Bierman, P.R., Rood, D.H., Neilson, T.B., Greene, E.S., Bower, J.A., Perdrial, N., 2017. Effects of grain size, mineralogy, and acid-extractable grain coatings on the distribution of the fallout radionuclides ^{7}Be, ^{10}Be, ^{137}Cs, and ^{210}Pb in river sediment. Geochim. Cosmochim. Acta 197, 71–86.
Sosa Gonzalez, V., Bierman, P.R., Nichols, K.K., Rood, D.H., 2016. Long-term erosion rates of Panamanian drainage basins determined using *in situ* ^{10}Be. Geomorphology.
Sosa Gonzalez, V., Schmidt, A.H., Bierman, P.R., Rood, D.H., 2017. Spatial and temporal replicability of meteoric and in situ ^{10}Be concentrations in fluvial sediment. Earth Surf. Process. Landf.
Stone, J., 1998. A rapid fusion method for separation of beryllium-10 from soils and silicates. Geochim. Cosmochim. Acta 62, 555–561.
Stone, J.O., 2000. Air pressure and cosmogenic isotope production. J. Geophys. Res. Solid Earth 105, 23753–23759.
Stone, J., Finnegan, N., Gendaszek, A., 2006. Playfair's law of beryllium-10. Geol. Soc. Am. Abstr. Programs 38.
Sutherland, D.G., Ball, M.H., Hilton, S.J., Lisle, T.E., 2002. Evolution of a landslide-induced sediment wave in the Navarro River, California. Geol. Soc. Am. Bull. 114, 1036–1048.
Syvitski, J.P.M., Vorosmarty, C.J., Kettner, A.J., Green, P., 2005. Impact of humans on the flux of terrestrial sediment to the global coastal ocean. Science 308, 376–380.
Vanacker, V., von Blanckenburg, F., Govers, G., Molina, A., Poesen, J., Deckers, J., Kubik, P., 2007. Restoring dense vegetation can slow mountain erosion to near natural benchmark levels. Geology 35, 303–306.
Von Blanckenburg, F., Hewawasam, T., Kubik, P.W., 2004. Cosmogenic nuclide evidence for low weathering and denudation in the wet, tropical highlands of Sri Lanka. J. Geophys. Res. Earth 109.
Walter, R.C., Merritts, D.J., 2008. Natural streams and the legacy of water-powered mills. Science 319, 299–304.
Willenbring, J.K., von Blanckenburg, F., 2010. Meteoric cosmogenic Beryllium-10 adsorbed to river sediment and soil: applications for Earth-surface dynamics. Earth Sci. Rev. 98, 105–122.
Wittmann, H., von Blanckenburg, F., 2016. The geological significance of cosmogenic nuclides in large lowland river basins. Earth Sci. Rev. 159, 118–141.
Wittmann, H., von Blanckenburg, F., Kruesmann, T., Norton, K.P., Kubik, P.W., 2007. Relation between rock uplift and denudation from cosmogenic nuclides in river sediment in the Central Alps of Switzerland. J. Geophys. Res. 112.
Wittmann, H., Von Blanckenburg, F., Guyot, J.-L., Maurice, L., Kubik, P., 2009. From source to sink: preserving the cosmogenic 10 Be-derived denudation rate signal of the Bolivian Andes in sediment of the Beni and Mamoré foreland basins. Earth Planet. Sci. Lett. 288, 463–474.
Wittmann, H., von Blanckenburg, F., Bouchez, J., Dannhaus, N., Naumann, R., Christl, M., Gaillardet, J., 2012. The dependence of meteoric ^{10}Be concentrations on particle size in Amazon River bed sediment and the extraction of reactive ^{10}Be/^{9}Be ratios. Chem. Geol. 318–319, 126–138.
Wittmann, H., Blanckenburg, F., Dannhaus, N., Bouchez, J., Gaillardet, J., Guyot, J.-L., Maurice, L., Roig, H., Filizola, N., Christl, M., 2015. A test of the cosmogenic ^{10}Be (meteoric)/^{9}Be proxy for simultaneously determining basin-wide erosion rates, denudation rates, and the degree of weathering in the Amazon basin. J. Geophys. Res. Earth 120, 2498–2528.
Xu, S., Dougans, A.B., Freeman, S.P.H.T., Schnabel, C., Wilcken, K.M., 2010. Improved ^{10B}e and ^{26}Al-AMS with a 5MV spectrometer. Nucl. Instrum. Methods Phys. Res., Sect. B 268, 736–738.
Xu, S., Freeman, S.P.H.T., Rood, D.H., Shanks, R.P., 2015. Decadal ^{10}Be, ^{26}Al and ^{36}Cl QA measurements on the SUERC 5 MV accelerator mass spectrometer. Nucl. Instrum. Methods Phys. Res., Sect. B 361, 39–42.